AKADÉMIAI KIADÓ

Pollack Periodica • An International Journal for Engineering and Information Sciences

18 (2023) 2, 84–89

DOI:
10.1556/606.2023.00760

ORIGINAL RESEARCH PAPER

Influence of class A40 autonomous truck on rutting and fatigue cracking

Mohammad Fahad* and Richard Nagy

Department of Transport Infrastructure and Water Resources Engineering, Faculty of Architecture, Civil Engineering and Transport Sciences, Széchenyi István University, Győr, Hungary

Received: November 18, 2022 • Revised manuscript received: February 3, 2023 • Accepted: February 20, 2023
Published online: May 18, 2023

ABSTRACT

Effects of autonomous trucks' different lateral wander modes have been analyzed in this research using a dload subroutine. Two lateral wander modes, a zero-wander mode in which a truck is programmed to follow a predetermined wheel path without any lateral movement and a uniform wander mode, where the truck uniformly distributes itself along the lateral width of the lane, are used. European class A40 truck has been modeled in ABAQUS code. Results show that fatigue life of pavement increases by 1.45 times if a uniform wander mode is used, which corresponds to a decrease in fatigue life of 14 months if a zero-wander mode is used. In case of rutting progression, 40% acceleration of rutting happens under a zero-wander mode. In case of uniform wander mode, rut depth decreases by 1.25 times against the zero-wander mode.

KEYWORDS

rutting, fatigue cracking, ABAQUS, autonomous trucks, lateral wander

1. INTRODUCTION

Autonomous Trucks (ATs) are bound to be integrated into the current transport infrastructure system, however for the initial period; ATs would be integrated with the current human driven truck traffic. Full segregation and coverage of autonomous trucks on highways requires a lot of refinement and training of artificial intelligence related to its behavior with the surrounding environment and vehicles. Effect of ATs on pavement structure requires in depth research since it is presumed that ATs will use the minimum width of lane without any lateral wander with the help of onboard sensors to increase fuel efficiency and traffic safety. However, under these zero lateral wander scenarios, an extensive amount of channelized loading can accelerate pavement distress and prematurely damage the pavement. In these research two lateral wander modes, a zero wander and a uniform wander mode are compared based on accumulated rutting by AT traffic.

Simulating the field conditions on asphalt pavement response requires using adequate modeling techniques. Pavement distress in terms of rutting induced by autonomous truck traffic can be measured using static and part dynamic loading scenarios as provided in ABAQUS code, however these methods are only limited to application where no lateral wander is considered in by traffic. Moreover, in another concept the moving load can be simulated by shifting the load and its amplitude over a loading path step by step until one wheel pass is completed [1, 2]. A dload subroutine written on FORTRAN code, on the other hand can be used to define position, time, element number and load integration point number being a function of distributed load magnitude. A dload subroutine can be used to define position, time and speed of applied load [3, 4].

Application of programmed scripts and dload subroutine integrated into ABAQUS has been evaluated in previous research. Si et al. [5] performed simulations of dynamic loading load on a pavement surface in a 3D model developed in ABAQUS by incorporating the dload

*Corresponding author.
E-mail: fahadmohammad854@gmail.com, fahad.mohammad@sze.hu

subroutine written in FORTRAN. Results concluded with good capability of suggested framework for indicating the progression of bottom-up cracking in pavement by self-sensing surface sensors. Cao et al. [6] employed the use of dload and ultra-cloud subroutines to simulate the moving load on bridge deck. Cheng et al. [7] used viscoelastic FE model developed in ABAQUS and performed dynamic loading analysis using a dload subroutine. Results showed that plastic behavior did not have impact of rutting; however the viscous behavior was the most prevalent one in occurrence of rutting.

2. RESEARCH METHODOLOGY

A typical four layered pavement structure has been selected consisting of an asphalt layer, aggregate base course, aggregate sub-base course, and a subgrade layer with presumed thickness of 2 m. Length of the pavement section to be analyzed is kept at 20 m and the width of the pavement section is kept at 3.5 m, simulating the width of truck traffic lane.

2.1. Pavement

Validated pavement layer properties to be used in ABAQUS have been taken from [8] as it shown in Table 1.

Furthermore, to include the viscoelastic behavior of asphalt mixture for permanent deformation calculation, Prony series parameters were used. Prony series parameters have previously been used to characterize the viscoelastic behavior of asphalt mixtures [9, 10]. Stress and strain relationship of a viscoelastic material can be described by Prony series that is a component of power law series. Time dependency of viscoelastic material in ABAQUS is described by the following Prony series expansion in Eqs (1) and (2),

$$g(t) = 1 - \sum_{t=1}^{N} g_i \left(1 - e^{t/\tau_i}\right), \tag{1}$$

$$g(t) = \frac{G(t)}{G(t=0)}, \tag{2}$$

where $g(t)$ is the ratio of shear modulus at time$t$; $G(t)$ is the shear modulus at $t = 0$, $G(t = 0)$; τ_i is the retardation time; and g_i is a Prony series coefficient. N is the number of terms in the Prony series. The value $g(t)$ can also be computed by normalizing $G(T)$ by G_0, which is the instantaneous shear modulus and $G(T)$ is obtained from relaxation modulus $E(t)$ from Eq. (3),

Table 1. Pavement layer properties

Layer type	Thickness (cm)	Elastic modulus (kPa)	Poissions ratio
Asphalt	20	950,000	0.41
Base course	40	500,000	0.35
Sub-base course	20	350,000	0.35
Subgrade	-	60,000	0.40

$$G(T) = \frac{E(t)}{2(1+\mu)}, \tag{3}$$

where μ is the Poisson's ratio and for the asphalt layer, a value of 0.35 is assumed. Finally, the series of retardation time is assumed and plugged into Eq. (1) and coefficients of Prony series are determined. The Prony series parameters in this research have been taken from [9] based on dynamic modulus testing on Hot Mix Asphalt (HMA) lab specimens as it shown in Table 2.

2.2. Loading

For the simulation of pavement loading, a typical European A40 type semi-truck with maximum allowable gross weight of 40 tones has been selected. Data from each axle has been obtained from [8] with axle configurations and axle loads is shown in Fig. 1

Tire contact pressure depends on a number of factors, for example, tire inflation pressure, tire load and its dimensions [11]. Since, the tire contact area varies with tire inflation pressure. Therefore, a term tire deflection introduced by [12] signifies the size of contact area and its dependence on tire inflation pressure. Significantly, at lower inflation pressures, tire deflection affects the increase in contact area size. The theoretical expression for tire deflection is given in Eq. (4),

$$\Delta = 0.008 + 0.001 \cdot \left(0.365 + \frac{170}{p_i}\right) \cdot G_k, \tag{4}$$

where, Δ is tire deflection (m); p_i is the tire inflation pressure (kPa); G_k is the wheel load (kN). Numerical expression of

Table 2. Prony series parameters

Elastic properties	
Poisson's ratio	Instantaneous modulus (MPa)
0.35	6,674
Prony constants	
Prony series coefficient g_i	Retardation time τ_i (sec)
0.611947	0.000063
0.251542	0.012589
0.068537	1.258925
0.030080	12.589254

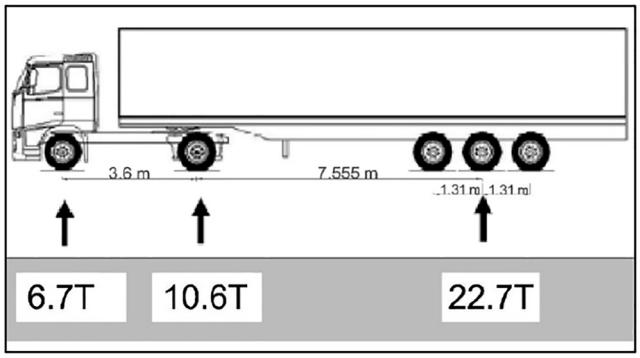

Fig. 1. Axle configuration, spacing and dimensions

Eq. (5) is used to calculate tire contact area, and Eq. (6) is used for calculating nominal tire contact pressure,

$$A = b^{0.8} \cdot d^{0.8} \cdot \Delta^{0.4}, \tag{5}$$

$$p = \frac{G}{b^{0.8} \cdot d^{0.8} \cdot \Delta^{0.4}}, \tag{6}$$

where, A is the contact area (m^2); G is the vehicle mass (kN); b is the width of unloaded wheel tire (m); d is the diameter of unloaded wheel tire (m). Furthermore, values of contact area and vertical tire contact pressure were further verified with results obtained from Moya et al. [13] for each tire load type and corresponding tire inflation pressure. Previous studies [14] have shown that the contact footprint of the tire is rectangular. A use of rather circular contact area can underestimate compressive strains on top of subgrade and overestimate the tensile strains at the bottom of asphalt layers [15]. Once the area is calculated, Eq. (7) taken from (6), is used to calculate longitudinal and lateral dimensions of the tire contact patch,

$$L = \sqrt{\frac{A_c}{0.5227}}, \tag{7}$$

where L is the constant that is used to measure longitudinal and lateral dimensions of contact patch using the values of 0.6 L and 0.8712 L respectively and A_c is the area of tire contact patch calculated from Eq. (5). Used tire type, inflation pressure and wheel load, tire contact pressure and contact patch length are shown in Table 3. Tire inflation pressure values were obtained from [16].

2.3. Finite element model

A 3D model has been developed with length of 20 m and width of 3.5 m. The total depth of the model is kept at 2.8 m and the bottom of the model has an interface of elastic foundation to simulate infinite thickness of natural soil foundation. Figure 2 shows the assembly of the model. Model type used is 8-node linear brick, reduced integration with hourglass control. Sensitivity analysis has been done for the element size selection based on the previous research conducted by [17]. Therefore, mesh of the model consisted of a total of 25,584 elements with an element size of 120 that has been validated.

The interaction of layers in the pavement was kept as a normal surface-to-surface contact with hard and frictionless characteristics. For the boundary conditions, nodes were free to move along the normal directions but were restricted in perpendicular horizontal directions as it is shown in Fig. 2.

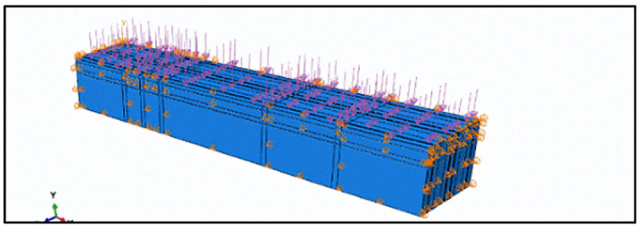

Fig. 2. Loading and boundary condition details

3. RESULTS AND DISCUSSION

Simulations have been conducted on ABAQUS using a dload subroutine where speed of the class A40 truck is kept constant at 90 km h^{-1} on a 20 m long pavement section. Simulations correspond to 5,000 average annual truck passes for a design life of 15 years.

Figure 3 shows the stress values exerted under each tire footprint while a truck is moving along the middle of the lane corresponding to the zero-wander mode at a moving speed of 90 km h^{-1}, highest stress accumulation within the truck axles is observed under the driving axle and along the middle axle of the trailer.

Furthermore, the stresses were recorded under the tires at various lateral positions of axles. Figure 4 shows the screenshot taken when the lateral positioning of the truck was at extreme left of the lane during a uniform wander mode.

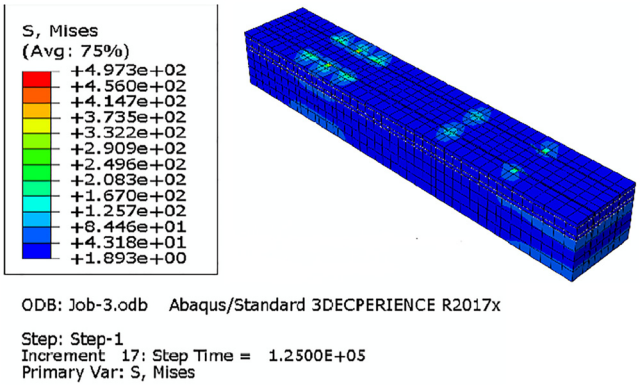

Fig. 3. Movement of truck as per a zero-wander mode

Table 3. Tire load, pressure, and dimensions

Tire type	295/80R22.5	295/80R22.5	385/65R22.5	385/65R22.5	385/65R22.5
Twin vs. Single	Single	Twin	Single	Single	Single
Axle load (Tons)	6.70	10.60	7.57	7.57	7.57
Load per wheel (kN)	32.85	25.98	37.00	37.00	37.00
Tire inflation pressure (kPa)	690	690	690	690	690
Tire contact pressure (kPa)	430	350	550	550	550
Contact patch Length/Width (mm)	250/330	250/310	275/310	275/310	275/310

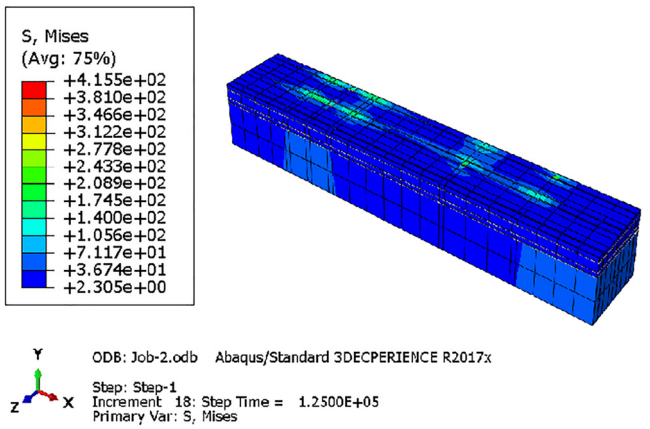

Fig. 4. Screenshot of truck tire stresses under a uniform wander mode

Magnitude of strain values were observed along the longitudinal profile under each axle and tire with raw data obtained from ABAQUS and are shown in Fig. 5. As observed with the total length of the section being 20 m. The highest magnitude of strains is recorded along the middle axle of the trailer at 350 μm, followed by the front and back axles of the trailer at 286 μm.

3.1. LEF and ESALs calculation

The damage accumulated from each axle corresponding to design life of 15 years was then converted into equivalent damage to a standard 80 kN single axle load using Load Equivalency Factor (LEF) [18]. A standard formula in which a standard single axle load of 80 kN is divided to a designated axle load and the ratio is powered to four in Eq. (8),

$$LEF = \left(\frac{\text{designated axle load}(kN)}{\text{standard axle load}(kN)}\right)^4. \tag{8}$$

A drive axle usually has a higher axle load of about 105.61 kN, hence the damage accumulated by this axle is three times that of damage accumulated by an 80 kN standard axle load. For the three single axles on the trailer, the damage from each axle was found to be equivalent to the standard axle load of 80 kN [19]. Hence, a total Equivalent Single AxLe to Truck (ESAL/Truck) ratio of 1.55 was obtained and was calculated using Eq. (9),

$$\text{Truck Category Esals in Construction Year} = \text{load factor} \cdot \text{Lane } AADT \cdot 3.65. \tag{9}$$

Table 4 shows the calculation of a construction year design ESALs.

Finally, total design ESALs are calculated in Eq. (10),

$$\text{Total design } ESALs = \text{total construciton year } ESALs \cdot \frac{(1 + i_{B\ to\ D})^n - 1}{i_{B\ to\ D}}, \tag{10}$$

where n is base year of construction and $i_{B\ to\ D}$ is growth rate from base year to final year of design period. With a growth rate of 3.5%, a total ESALs of 1,300,000 were obtained.

The calculated vertical strain values under the top of subgrade were eventually reduced to a corresponding amount and it is shown in Fig. 6.

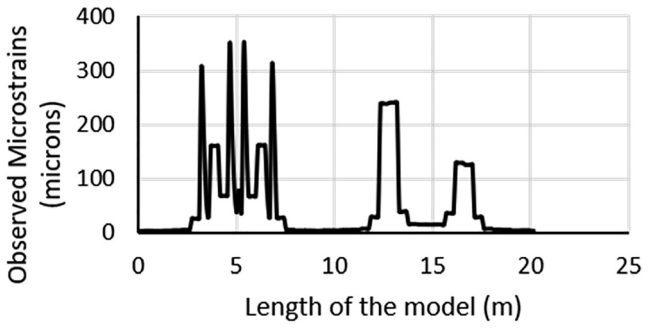

Fig. 5. Strain recorded along the longitudinal profile

3.2. Rutting and fatigue cracking evaluation

Using the equivalent values of micro-strains observed with a projected traffic of 1.3 million ESALs for a design life of 15 years, number of loading cycles to rutting and fatigue cracking were calculated from the distress prediction models developed by Asphalt Institute. Two of the fatigue and rutting prediction models respectively given by Asphalt Institute are presented in Eqs. (11) and (12) respectively [20],

$$N_f = 0.0796 \cdot \varepsilon_c^{-3.291} \cdot E^{-0.854}, \tag{11}$$

$$N_d = 1.365 \cdot 10^{-9} \cdot \varepsilon_t^{-4.477}, \tag{12}$$

Fig. 6. Comparison of strains under the longitudinal profile for zero wander and uniform wander modes

Table 4. Construction year ESALs

Truck Category	Load Factor (ESALs/Truck)	Lane Average Annual Daily Traffic	ESALs in construction Year
5 Axles	5.88	5,000	29,400

Fig. 7. Measured rut depth at 1.3 million ESALs

where N_f is the allowable number of load repetitions to prevent fatigue cracking and N_d is the allowable number of load repetitions to prevent permanent deformation (rutting); E is the elastic modulus of asphalt concrete layer; ε_t is horizontal tensile strain under HMA layer and ε_c is vertical compressive strain on top of the subgrade.

Micro-strains obtained from FE modeling are used to calculate permanent plastic strain ε_p as per following using Eq. (13), [21],

$$\varepsilon_p = \varepsilon_r \cdot a_1 \cdot N^{a_2} \cdot T^{a_3}, \tag{13}$$

where ε_p is the permanent strain; ε_r is the resilient strain; N is the number of load repetitions; T is the temperature and a_1, a_2, a_3 are the regression coefficients with values 1.69, 1.85, 0.275 respectively, taken from [22]. Finally, the rut depth occurring in asphalt layer can be computed using the following Eq. (14), [23],

$$RD = \sum_{I=1}^{N} \varepsilon_P^I h^i, \tag{14}$$

where RD is the total rut depth in the asphalt concrete layer; N is the number of sublayers; ε_P^I is the plastic strain in the ith sublayer; and h^i is the thickness of the i-th sub-layer.

Rut depth was obtained using equation and also compared from the (U) deformation results in ABAQUS results section and presented in Fig. 7. With projected traffic of 1.3 million ESALs the pavement reaches a rut depth of 10.21 mm at the end of its service life.

4. CONCLUSIONS AND FINDINGS

In this research, a fully loaded class A40 truck with maximum allowable weight of 40 kN has been used to analyze the effect of zero wander and uniform wander modes on resulting fatigue life and magnitude of rut depth in the flexible pavement. Moving load has been simulated by using the dload subroutine written in FORTRAN.

A difference in magnitude of rut depth is 1.5 times lower and fatigue life can increase by a factor of 40% if a uniform wander mode is used, making the uniform wander mode an ideal selection for lateral wander of autonomous trucks. In terms of limitations, effects of temperature and climatic conditions have not been taken into account. Therefore, pavement performance would be favorable for resistance against fatigue during lower temperatures and favorable against rutting during higher temperatures.

Following findings are obtained from this research.

1. Due to action of induced vertical strains, decrease in fatigue life is around 1.75 times more in case of a zero wander mode;
2. Fatigue life decreases by 14 months in case of a zero wander mode;
3. A rutting depth of 6 mm occurs under a uniform wander mode at about 1,105,380 number of passes which roughly translates to 8 percent advancement of rutting progression near the end of service life of pavement;
4. Overlap of wheel paths occurs in case of uniform wander mode, with the overlapping width of 1.5 m for an A40 type truck;
5. Acceleration for rut development in case of a zero wander is almost 2 times than that of a uniform wander mode;
6. After the end of service life of pavement, under zero wander mode, rut depth is around 10 mm.

REFERENCES

[1] A. H. Alavi, H. Hasni, N. Lajnef, and K. Chatti, "Continuous health monitoring of pavement systems using smart sensing technology," *Constr. Build. Mater.*, vol. 114, pp. 719–736, 2016.

[2] P. Penmetsa, E. K. Adanu, D. Wood, T. Wang, and S. L. Jones, "Perceptions and expectations of autonomous vehicles - A snapshot of vulnerable road user opinion," *Technol. Forecast. Soc. Change.*, vol. 143, pp. 9–13, 2019.

[3] Y. Chen, H. Zhang, X. Q. Zhu, and D. W. Liu, "The response of pavement to the multi-axle vehicle dynamic load," in *Proc. Int. Conf. Electr. Autom. Mech. Eng.*, Jiaxing, China, March 12–12, 2015, pp. 238–241.

[4] E. Juhasz and S. Fischer, "Investigation of railroad ballast particle breakage," *Pollack Period.*, vol. 14, no. 2, pp. 3–14, 2019.

[5] N. Lajnef, K. Chatti, H. Hasni, and A. H. Alavi, "Feasibility of early damage detection using surface mounted sensors on existing pavements," Technical report no. CHPP Report-MSU#4-2018, Michigan State University, 2016.

[6] C. Si, H. Cao, E. Chen, Z. You, R. Tian, R. Zhang, and J. Gao, "Dynamic response analysis of rutting resistance performance of high modulus asphalt concrete pavement," *Appl. Sci.*, vol. 8, no. 12, 2018, Paper no. 2701.

[7] P. Cao, D. C. Feng, and R. X. Jing, "Based on FE method to research resistant rutting ability of pavement structure in Heilongjiang province," *Appl. Mech. Mater.*, vol. 128, no. 129, pp. 1349–1354, 2012.

[8] Z. A. Alkaissi and Y. M. Al-Badran, "Finite element modeling of rutting for flexible pavement," *J. Eng. Sustain. Dev.*, vol. 22, no. 3, pp. 1–13, 2018.

[9] M. Ghorban Ebrahimi, M. Saleh, and M. A. M. Gonzalez, "Interconversion between viscoelastic functions using the Tikhonov regularisation method and its comparison with approximate techniques," *Road Mater. Pavement Des.*, vol. 15, no. 4, pp. 820–840, 2014.

[10] H. Alimohammadi, J. Zheng, A. Buss, V. R. Schaefer, C. Williams, and G. Zheng, "Finite element viscoelastic simulations of rutting behavior of hot mix and warm mix asphalt overlay on flexible pavements," *Int. J. Pavement Res. Technol.*, vol. 14, no. 6, pp. 708–719, 2021.

[11] A. Mansourkhaki, S. Yeganeh, and A. Sarkar, "Numerical comparison of pavement distress due to moving load under dual-wheel tandem and tridem axles," *Int. J. Transp. Eng.*, vol. 2, no. 1, pp. 31–46, 2014.

[12] P. B. Filho, H. Raymundo, S. T. Machado, A. R. C. A. P. Leite, and J. B. Sacomano, "Configurations of tire pressure on the pavement for commercial vehicles: Calculation of the 'n' number and the consequences on pavement performance," *Indep. J. Manag. Prod.*, vol. 7, no. 5, pp. 584–605, 2016.

[13] J. P. Aguiar-Moya, A. Vargas-Nordcbeck, F. Leiva-Villacorta, and L. G. Loría-Salazar, Eds, *The Roles of Accelerated Pavement Testing in Pavement Sustainability*, Springer, 2016.

[14] M. Guo, X. Li, M. Ran, X. Zhou, and Y. Yan, "Analysis of contact stresses and rolling resistance of truck-bus tyres under different working conditions," *Sustain.*, vol. 12, no. 24, pp. 1–16, 2020.

[15] H. Wang and M. Li, "Comparative study of asphalt pavement responses under FWD and moving vehicular loading," *J. Transp. Eng.*, vol. 142, no. 12, pp. 6–17, 2016.

[16] X. Tang, J. Xie, H. Xie, and H. Zhang, "Predictions of three-dimensional contact stresses of a radial truck tire under different driving modes," *Adv. Mech. Eng.*, vol. 14, no. 4, pp. 1–18, 2022.

[17] M. Fahad, R. Nagy, and P. Fuleki, "Creep model to determine rut development by autonomous truck axles on pavement," *Pollack Period.*, vol. 17, no. 1, pp. 1–6, 2021.

[18] G. Leonardi, "Finite element analysis for airfield asphalt pavements rutting prediction," *Bull. Polish Acad. Sci. Tech. Sci.*, vol. 63, no. 2, pp. 397–403, 2015.

[19] S. I. R. Amorim, J. C. Pais, A. C. Vale, and M. J. C. Minhoto, "A model for equivalent axle load factors," *Int. J. Pavement Eng.*, vol. 16, no. 10, pp. 881–893, 2015.

[20] F. Salour and S. Erlingsson, "Investigation of a pavement structural behaviour during spring thaw using falling weight deflectometer," *Road Mater. Pavement Des.*, vol. 14, no. 1, pp. 141–158, 2013.

[21] A. D. Mwanza, M. Muya, and P. Hao, "Towards modeling rutting for asphalt pavements in hot climates," *J. Civ. Eng. Archit.*, vol. 10, no. 9, pp. 1075–1084, 2016.

[22] M. A. T. Romero, M. D. Gomez, and L. E. L. Uribe, "Prony series calculation for viscoelastic behavior modeling of structural adhesives from DMA data," *Ing. Investig. y Tecnol.*, vol. 21, no. 2, pp. 1–10, 2020.

[23] Y. Deng, X. Shi, Y. Zhang, and J. Chen, "Numerical modelling of rutting performance of asphalt concrete pavement containing phase change material," *Eng. Comput.*, vol. 11, no. 6, pp. 39–55, 2021.